Available online at www.sciencedirect.com
ScienceDirect
International Journal of Heat and Mass Transfer 50 (2007) 3890–3898
International Journal of HEAT and MASS TRANSFER
www.elsevier.com/locate/ijhmt

Development of optical naphthalene sublimation method

Kiho Hong, Tae-Ho Song *

Department of Mechanical Engineering, Korea Advanced Institute of Science and Technology, Kusong-dong 373-1, Yuseong-gu, Daejon, South Korea

Received 24 September 2006; received in revised form 3 February 2007
Available online 16 April 2007

Abstract

The naphthalene sublimation technique is one of the most convenient mass transfer methods to determine local heat transfer coefficient by using the heat and mass transfer analogy; however, it has difficulties in molding the naphthalene and measuring the naphthalene thickness in arbitrary shapes. This study introduces a new naphthalene thickness measurement technique using an optical method to be applied to arbitrary shapes. Naphthalene coating is made on an arbitrarily-shaped glass substrate using vapor plating. Later, collimated laser light is illuminated onto it and a CCD camera detects the scattered light to measure the thickness before and after the sublimation process. The correlations between the naphthalene thickness and the signal strength of the CCD image are preliminarily found. With the correlations, four wind tunnel experiments with flat plate, wedge, plate-wedge and cylinder flow are performed. The results demonstrate the capability of accurately measuring the naphthalene thickness in a fast optical manner, which eventually enables a more universal naphthalene sublimation technique.

1. Introduction

In many experimental heat transfer problems, local heat transfer coefficient is measured with great difficulty together with complicated experimental equipment. A novel method to get the local convective heat transfer coefficient is to perform a mass transfer experiment instead [13]. This technique employs the analogy between the local heat and mass transfer coefficients. The mass transfer results are converted to heat transfer outputs using the following steps:

(i) make the naphthalene test specimens;
(ii) measure the initial naphthalene surface profile or the weight;
(iii) make an experiment with the naphthalene specimens;
(iv) measure again the naphthalene surface profile or the weight;
(v) calculate the Sherwood number.

Making naphthalene coatings can be done in several ways; molding, dipping, spraying, machining, and so on. Saboya and Sparrow [1] use the naphthalene mass transfer method to measure the local coefficient for heat exchangers. They make the naphthalene layer by molding. Chyu [2] coat the test piece by dipping it into a beaker of liquid naphthalene when many small pieces such as pin–fin arrays are needed. Neal and co-workers [3,4] and Lee [5,6] have developed spray method. Sparrow and Ramsey [7] fabricate naphthalene blocks by machining which can make multiple specimens of identical size and smooth surfaces of naphthalene. Zhang [8] cast out the naphthalene to simulate flat tube bank. Park and Yoo [9] study with naphthalene casting facility and LVDT (Linear Variable Differential Transformer) for flow over a flat plate. Kim [10] adopts the naphthalene molding and measure the naphthalene thickness using LVDT.

When using coating method, it is essential to make the original substrate surface and to measure the naphthalene thickness accurately. Usually, the naphthalene thickness is measured by LVDT that makes direct contact to the naphthalene surface. This has a limitation that it is not

* Corresponding author. Tel.: +82 42 869 3032; fax: +82 42 869 3210.
E-mail address: thsong@kaist.ac.kr (T.-H. Song).

0017-9310/$ - see front matter © 2007 Elsevier Ltd. All rights reserved.
doi:10.1016/j.ijheatmasstransfer.2007.02.017

Nomenclature

D	cylinder diameter, m
D_N	diffusion coefficient of naphthalene in air, m^2/s
h	heat transfer coefficient, W/m^2 K
h_m	mass transfer coefficient, m/s
I	light intensity
k	thermal conductivity, W/m K
$\dot{m}''$	sublimation mass flux, kg/m^2 s
$\dot{M}$	total mass flow rate of sublimated naphthalene, kg/s
Nu	the Nusselt number
Pr	the Prandtl number
$\dot{Q}$	volume flow rate of air, m^3/s
Re_D	the Reynolds number
Sc	the Schmidt number
Sh_D	the Sherwood number
t	naphthalene thickness, μm
U	velocity of air, m/s
x	coordinates along the air flow, m
y	coordinates transverse to the air flow, m
z	vertical coordinates, m

Greek symbols

α	thermal diffusivity, m^2/s
v	kinematic viscosity, m^2/s
τ	naphthalene sublimation depth, m
β	total angel of wedge, deg
λ	wavelength of laser light, nm
θ	light incidence angle, deg
ρ	density, kg/m^3
ρ_s	density of solid naphthalene, kg/m^3
ρ_{sat}	saturation density of naphthalene vapor, kg/m^3
ρ_{bulk}	bulk density of naphthalene in the air, kg/m^3
ϖ_N	mass fraction of naphthalene in the air

Subscripts

b	bulk
inf	infinite
m	mass, mean
N	naphthalene
o	reference
s	surface, solid
sat	saturated

applicable to complicated geometries not to mention the difficulty of making the specimens.

The present study introduces a new method to circumvent these obstacles; the optical naphthalene sublimation technique makes complex-shape experiments possible. The process is composed of coating naphthalene on a complicated-shape plate and using an optical method for the naphthalene thickness measurement. Correlations between the naphthalene thickness and the signal strength from the optical detector are preliminarily found. The sublimated thickness is actually measured with the correlation as will be detailed and demonstrated.

2. The optical naphthalene sublimation method

2.1. Background

The naphthalene sublimation technique is based on the fact that there is a mathematical analogy between the energy equation and the species equation. Temperature T and thermal diffusivity α in the energy equation are replaced with the mass fraction of naphthalene ω_N and diffusion coefficient D_N of naphthalene in air in the species one. These equations are non-dimensionalized like followings:

$$u^*\frac{\partial T^*}{\partial x^*}+v^*\frac{\partial T^*}{\partial y^*}+w^*\frac{\partial T^*}{\partial z^*}=\frac{1}{Re_D Pr}\left(\frac{\partial^2 T^*}{\partial x^{*2}}+\frac{\partial^2 T^*}{\partial y^{*2}}+\frac{\partial^2 T^*}{\partial z^{*2}}\right) \tag{1}$$

$$u^*\frac{\partial \omega_N^*}{\partial x^*}+v^*\frac{\partial \omega_N^*}{\partial y^*}+w^*\frac{\partial \omega_N^*}{\partial z^*}=\frac{1}{Re_D Sc}\left(\frac{\partial^2 \omega_N^*}{\partial x^{*2}}+\frac{\partial^2 \omega_N^*}{\partial y^{*2}}+\frac{\partial^2 \omega_N^*}{\partial z^{*2}}\right) \tag{2}$$

These are non-dimensionalized using a typical length and the representative velocity U of air, respectively. As the result, the following dimensionless parameters, i.e., the Reynolds number Re_D, the Prandtl number Pr and the Schmidt number Sc are defined.

$$Re_D=\frac{UD}{v} \tag{3}$$

$$Pr=\frac{v}{\alpha} \tag{4}$$

$$Sc=\frac{v}{D_N} \tag{5}$$

In the above definitions, v is the kinematic viscosity of the air and D_N is the binary diffusion coefficient for naphthalene vapor in air. If the Prandtl and the Schmidt numbers are the same in the same flow configuration, the two dimensionless variables have exactly same values. Consequently, if the mass transfer relation is obtained by an experimental method, the heat transfer relation can be deduced from the other.

In the naphthalene sublimation method, the Sherwood number, defined as Eq. (6), is measured, which is the counterpart of the Nusselt number in the heat transfer.

$$Sh_D=\frac{h_m D}{D_N} \tag{6}$$

$$Nu_D = \frac{hD}{k} \tag{7}$$

where h_m, h and k are the mass transfer coefficient, the heat transfer coefficient and the thermal conductivity, respectively. From this analogy, we can identify the Nusselt number as the Sherwood number when the Prandtl number is the same as the Schmidt number. Actually, these two numbers, Pr and Sc, are not same in practice. Instead, we can use the following approximate relation in obtaining the Nusselt number.

$$Nu_D = Sh_D\left(\frac{Pr}{Sc}\right)^n \tag{8}$$

The power n is varied from 0.3 to 0.4 according to whether the flow is heated or cooled and to which geometry is under consideration [13].

The local mass flux $\dot{m}''$ at each location is calculated from the following expression:

$$\dot{m}''(x,y) = \rho_s \frac{\tau(x,y)}{\Delta t}, \tag{9}$$

where ρ_s is the density of solid naphthalene, τ is the local sublimation depth, and Δt is the blowing time. The thermophysical properties of naphthalene, as well as the saturation vapor pressure, are obtained from Goldstein and Cho [11]. The local mass transfer coefficient h_m can then be calculated as follows:

$$h_m(x,y) = \frac{\dot{m}''(x,y)}{\rho_{sat} - \rho_{bulk}(x)}, \tag{10}$$

where ρ_{sat} is the saturation vapor density of naphthalene and represents the density of naphthalene vapor at the wall, and ρ_{bulk} is the bulk density of naphthalene vapor in the local airflow passing through the cross section at a fixed x-coordinate. The saturation vapor density can be evaluated from the saturation vapor pressure and the perfect gas law, and the bulk density can be evaluated as

$$\rho_{bulk}(x) = \rho_{bulk}(0) + \frac{\dot{M}(x)}{\dot{Q}} \tag{11}$$

where $\dot{Q}$ is the volume flow rate passing through the test section and $\dot{M}(x)$ is the rate of total mass transfer from the plates. Since $\rho_{bulk}(0) = 0$ and $\dot{M}(x)$ is given by

$$\dot{M}(x) = \int_0^x \int_0^y \dot{m}''(x',y')\mathrm{d}y'\mathrm{d}x' \tag{12}$$

the local mass transfer coefficient h_m is finally expressed as

$$h_m(x,y) = \frac{\dot{m}''(x,y)}{\rho_{sat} - \frac{1}{\dot{Q}}\int_0^x \int_0^y \dot{m}''(x',y')\mathrm{d}y'\mathrm{d}x'} \tag{13}$$

Finally, the local Sherwood number Sh_D is calculated by Eq. (6).

2.2. Naphthalene vapor deposition technique

Casting is the most popular method of making the naphthalene. However, it is unsuitable to thin and complicated geometry. We present a new coating technique using vapor deposition, where the naphthalene vapor deposits onto the test plate under a moderate vacuum condition.

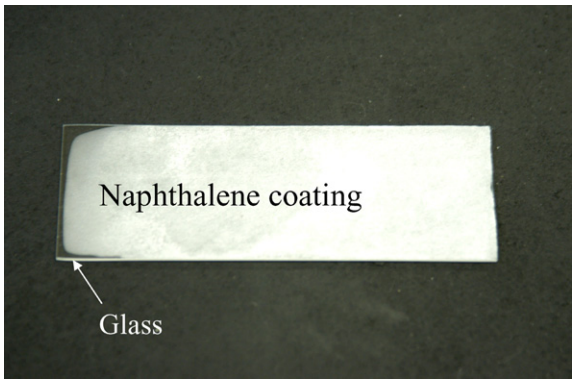

Fig. 1. Naphthalene coating.

First, a beaker (bore 66 cm and volume 250 ml in this experiment) is filled with naphthalene and it is heated using a hot-plate to the boiling point (217 °C) to generate naphthalene vapor. The beaker is then removed from the hot-plate and naphthalene liquid (200 ml) is allowed to cool down. When the naphthalene liquid temperature drops to 180 °C, it is put into a vacuum chamber at 150 Torr and room temperature. Glass substrate in the form of the test geometry is placed on the beaker for the vapor to stick onto it to form a solid coating. Both beaker and glass substrate are adhered closely for the naphthalene vapor not to leak. After a sufficient of time of 5–15 min, it is removed from the chamber.

Naphthalene coating thickness depends on the solidification time in the chamber. The more time elapses, the thicker naphthalene layer is formed. Coating thickness varies from 20 to 80 μm and has a very smooth surface. A typical vapor coating is shown in Fig. 1. Substrate is a 1 mm thick glass and the white part is the naphthalene coatings with 40 μm thickness. To evaluate uniformity of the naphthalene surface, we measured the reference naphthalene specimen thickness using LVDT. It is very uniform and naphthalene thickness is 0.047 ± 0.0005 mm with precision error 1.2% at a 95% confidence level. We also examine the coating surfaces under a microscope with a magnification

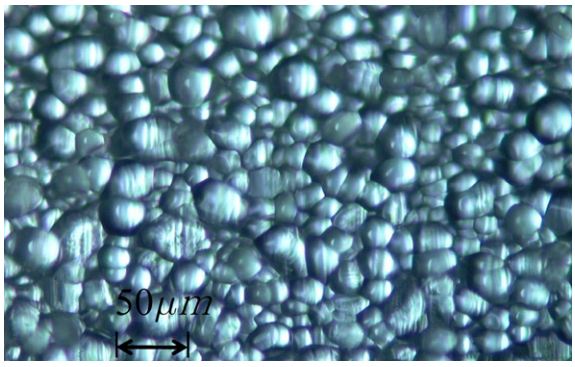

Fig. 2. Microphotograph of naphthalene coating with magnification factor of 200.

factor of 200. As shown in Fig. 2, coating layer consists of naphthalene grains whose size varies from 15 to 25 μm. The grains are in monoclinic lattice structure, with finer grain size near the substrate than near the surface. The coating thickness is easily handled by varying the deposition time. It is satisfactory if the naphthalene coating layer have a uniform thickness.

3. Experimental method

The basic idea of naphthalene thickness measurement is to illuminate the film with a laser and correlate the image strength to the local thickness. In naphthalene, the absorptance of light decreases and the transmissivity increases as the light wavelength increases. The surface reflection of light is uniform up to $\lambda = 700$ nm. When a He–Ne laser (632.8 nm wavelength) illuminates the naphthalene coating, some part of the light is reflected either by the surface or by scattering, some transmitted, and the other absorbed. Magnitudes of layer absorptance and transmissivity are relatively smaller than that of scattering due to reflection at the grain-to-grain boundaries. This scattered light goes in all directions when it comes out at the back side of naphthalene surface. If the naphthalene coating is thicker, the light detected behind the naphthalene coating decreases mainly because of the scattering.

We can detect the signal light in many different ways. First, the reflection by the naphthalene layer is detected. If the naphthalene is coated on total reflection material, i.e., well-polished aluminum, some part of the light is reflected at the surface, some scattered at the grain boundaries, some transmitted in naphthalene, then reflected by the substrate surface and comes out at the naphthalene surface. To detect the reflected light, a photo-detector may be perpendicularly placed above the naphthalene coating. The signals then depend on the incidence angle of the light and the naphthalene thickness.

The other way is to detect the reflected light behind the naphthalene coating on a transparent substrate such as glass. Detector measures the transmitted light behind the naphthalene coating. We employ this practice in this research.

Experiment is performed to find the correlations between the naphthalene thickness and the light intensity detected at the back of coating. The experimental apparatus is shown schematically in Fig. 3. A He–Ne laser beam (20 mW) is used to make a collimated beam. To expand laser beam uniformly, spatial filler is used. The path of laser beam is increased by mirrors and thus spatialy expanded. Since the laser light has a Gaussian distribution, we use the central part of the beam to form a collimated light at the naphthalene coating through iris and concave mirror. Then the beam power is significantly reduced to 3 μW. The stepping motor gives incidence angle variation to accept various naphthalene surface configurations. It can change the incidence angle every 10°. The image capturing board and computer saves the image taken by the

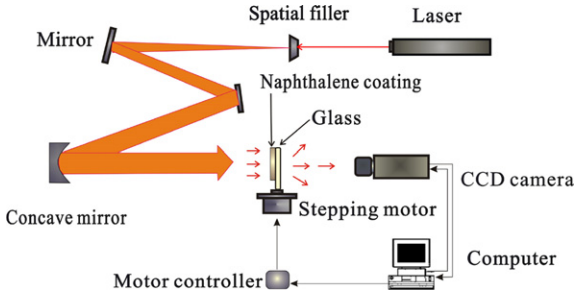

Fig. 3. Schematic diagram of the optical experimental apparatus.

CCD camera as TIFF file format. The CCD camera (KODAK) has a resolution of 1 K × 1 K pixels. The image capturing board is EPIX's XCAP and the CCD camera exposure time is 20 ms.

The TIFF file has data in the form of RGB colors. Since we use a 632.8 nm wavelength, we extract red part from the images through the image board. It has the information of light intensity and can be converted into ASCII code in the combination from 0 to 256. Pixel averaging is conducted to obtain light intensity with 20 × 20 pixels which correspond to 1 mm × 1 mm spatial resolutions, which again contains a few thousand grains.

To check the accuracy of the correlation, we conduct an uncertainty analysis. The measurement error consists of bias error and precision error. The uncertainty U of a general quantity is given as follows [14]:

$$U = (B^2 + P^2)^{1/2}, \tag{14}$$

where B and P are the bias and the precision uncertainties, respectively. The instrumentation bias error B is negligible is this study, thus set to be zero. The precision uncertainty is determined by

$$P = t_{95\%,v}\frac{S}{\sqrt{N}} \tag{15}$$

$$v = N - 1 \tag{16}$$

$$S = \sqrt{\frac{1}{N}\sum_{i=1}^{N}(x_i - \bar{x})^2} \tag{17}$$

where, $t_{95\%,v}$, S, v, N, $\bar{x}$ and x_i are t-distribution for a confidence level of 95%, standard deviation, degree of freedom, number of data, sample mean and measured values of a particular experiment. The total uncertainty δR of a derived quantity R as a function of $v_1, v_2, \ldots, v_n$ (i.e., $R = f(v_1, v_2, \ldots, v_n)$) can be estimated using [17]:

$$\frac{\delta R}{R} = \sqrt{\left\{\frac{\delta v_1}{v_1}\right\}^2 + \left\{\frac{\delta v_2}{v_2}\right\}^2 + \ldots + \left\{\frac{\delta v_n}{v_n}\right\}^2} \tag{18}$$

To analyze the uncertainty for the mass transfer coefficient h_m, the uncertainty dh_m can be expressed as

$$(dh_m)^2 = \left(\frac{\partial h_m}{\partial \tau}d\tau\right)^2 + \left(\frac{\partial h_m}{\partial \rho_{sat}}d\rho_{sat}\right)^2 + \left(\frac{\partial h_m}{\partial \rho_s}d\rho_s\right)^2 \tag{19}$$

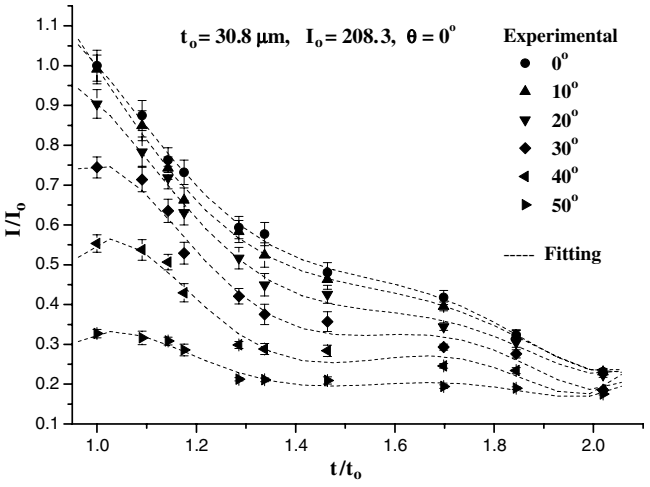

Fig. 4. The experimental results.

Table 1
Polynominal coefficients of a_{ij}

j	i					
	0	1	2	3	4	5
0	−37.38	146.78	−215.04	151.71	−52.03	6.97
1	279.48	−958.81	1297.48	−866.44	285.51	−37.15
2	−1277.64	4014.21	4370.97	3914.04	−1281.37	165.54
3	1085.56	−3678.14	−3729.69	−3350.77	1097.07	−141.65

or,

$$\left(\frac{\mathrm{d}h_{\mathrm{m}}}{h_{\mathrm{m}}}\right)^2 = \left(\frac{\mathrm{d}\tau}{\tau}\right)^2 + \left(\frac{\mathrm{d}\rho_{\mathrm{sat}}}{\rho_{\mathrm{sat}}}\right)^2 + \left(\frac{\mathrm{d}\rho_{\mathrm{s}}}{\rho_{\mathrm{s}}}\right)^2 \tag{20}$$

The uncertainty of sublimation depth τusing optical method is 8.5% including 3.8% fitting error and 7.65% reading error at a 95% confidence level. Also, using the relevant data, the uncertainties, ρ_{sat} and ρ_{s} are 3.9% [10] and 1.1% [11] respectively. Comprising all these uncertainties in Eq. (20), the total uncertainty in h_{m} is 9.3%.

Fig. 4 shows the results of image intensity for the naphthalene thickness at various incidence angles. As can be seen from the figure, the light intensity decreases when the incidence angle is large and the coating is thick. The correlation can be obtained in a polynomial as follows:

$$\frac{I}{I_{\mathrm{o}}} = \sum_{i=0}^{5}\sum_{j=0}^{3} a_{nm}\theta^m (t/t_{\mathrm{o}})^n, \quad t_0 = 30.8\ \mu\mathrm{m},\ I_{\mathrm{o}} \text{ at } \theta = 0^\circ, \tag{21}$$

where a_{ij} is the coefficients as shown Table 1. A few unrealistic inflection points are found in the fitted curves, and the error of this correlation is ±3.8%. It is the percent relative error between actual measurement point and fitting point with a polynomial form.

4. Experimental verifications

Wind tunnel experiments are performed to verify the proposed optical method. An open-loop wind tunnel with a suction blower is usually recommended for naphthalene sublimation experiments. As shown in Fig. 5, a low-speed open-loop wind tunnel having a cross-section 0.15 m × 0.15 m is used in this study. The wind tunnel is equipped with a 0.75 kW variable revolution blower that provides a maximum speed of approximately 1.5 m/s and the test section is located in the upstream of the blower having maximum flow rate of 3.3 m^3/min. It is important to maintain a precise temperature during the naphthalene experiments because the saturation vapor pressure of naphthalene and thus the mass diffusion coefficient are very sensitive to the temperature [11]. The wind tunnel experiments are carried out in a constant temperature humidity chamber with a size of 2.3 m × 1.8 m × 2.3 m and the temperature range from −30 °C to 80 °C.

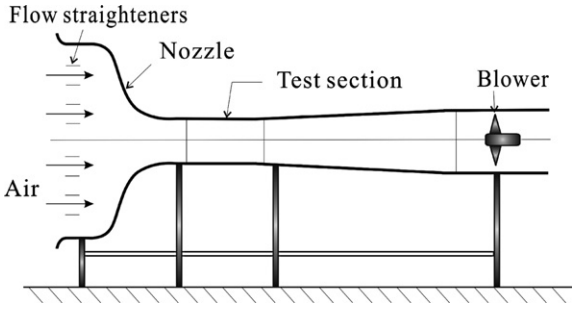

Fig. 5. Schematic diagram of the wind tunnel.

The first experiment in this study is the well known case of flow over a flat plate. This is performed since it can be used as a benchmark case to check to the accuracy of the naphthalene thickness measurement. After obtaining naphthalene coating on a glass substrate by the aforementioned vapor plating, the CCD images are taken. The glass substrate with a length of 5 cm is put into the test section of the wind tunnel. Sublimation is performed for 5400 seconds at 15 °C, *RH* 30% and 0.63 m/s of free stream velocity. The diffusion coefficient of naphthalene in air is

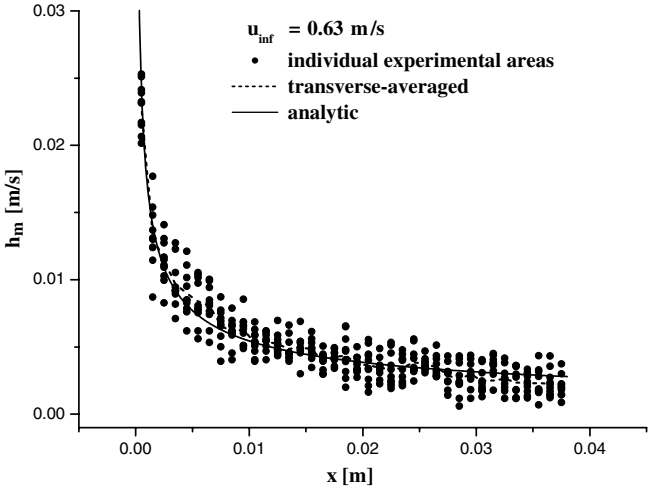

Fig. 6. Comparison between the experimental results and the analytic solutions for flat plate flow.

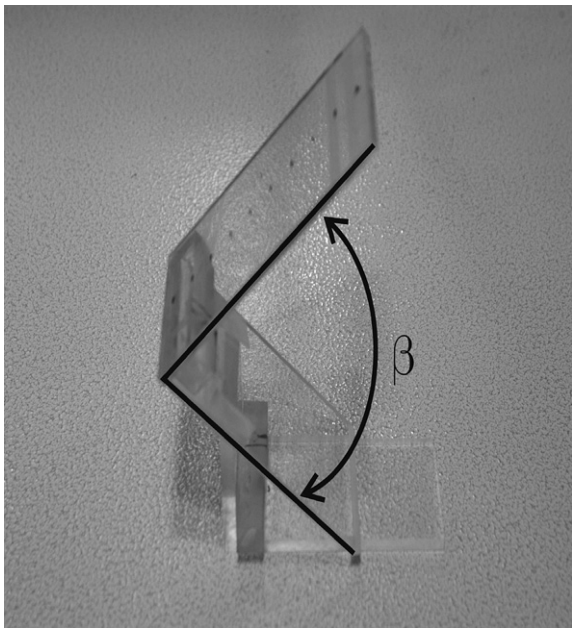

Fig. 7. Substrate of wedge flow.

6.4×10^{-6} m^2/s and the Schmidt number is 2.291. The sublimation thickness is varied from 0.5 μm to 7 μm. After the sublimation process, images are taken again. By calculating the naphthalene thickness change before and after the sublimation process, the mass transfer coefficient can be obtained.

The Blasius solution is taken as the reference exact solution. Comparison with the exact solution and the experimental results is shown in Fig. 6. Note that there are nine sampling area measurements at an x-location. The transverse-averaged results are in good agreement with the exact solution with fairly high individual scatter at an x-location. The total uncertainty of experimental precision error of the transverse-averaged data is 9.7% associated with 95% confidence. This means that a few thousand grains contained in a spatial sampling area (1 mm × 1 mm) do not reveal the average mass transfer coefficient accurately while averaging over the nine transverse areas gives highly accurate results. Considering that usually, 9 times more sampling does not significantly improves statistical accuracy for random sample, it is clear that the grains in

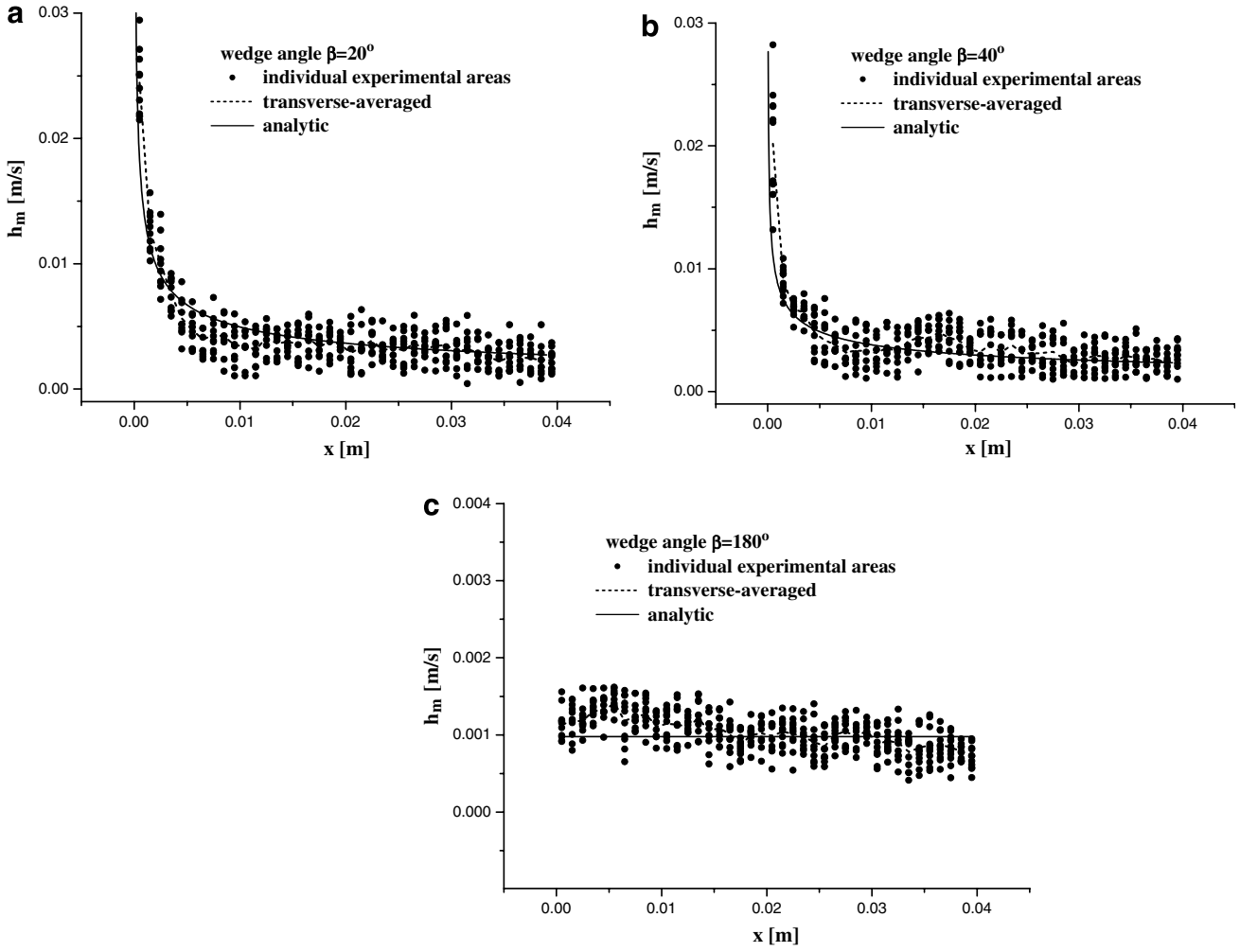

Fig. 8. Comparison between the experimental results and the analytic solutions for wedge flow. (a) Total angle of the wedge $\beta = 20°$, (b) total angle of the wedge $\beta = 40°$, (c) total angle of the wedge $\beta = 180°$.

close vicinities are not optically random but highly correlated. Indeed, closer grains are aligned in similar directions, resulting in visible speckles of size of hundreds or thousand of grains. It is appropriate here to mention why the individual data scatter so much in spite of the good agreement for the transverse-averaged data. Each grain in the layer is randomly aligned and the transmission of light through a straight line in the layer is heavily dependent on the local grain alignment. Moreover, neighboring grains tend to align in the same direction. Magnified view of the layer reveals that up to thousands of grains in a vicinity of 1 mm × 1 mm area align in the almost same direction. This is why each individual data are highly scattered; averaging over sufficiently for areas is needed for good accuracy.

The second experiment is for a wedge flow. As shown in Fig. 7, a substrate of wedge-shape is made at first. A glass of wedge shape is coated with naphthalene and the sublimation experiment is conducted in the same way as in the flat plate case. The boundary layer equations are solved by a shooting method. The experimental conditions are the same as in the flat plate case. Fig. 8 shows the experimental results compared with the analytic solution. As can be seen, the experimental results of both 20° and 40° are similar to that of flat plate flow. The overall uncertainty is 9.3% when

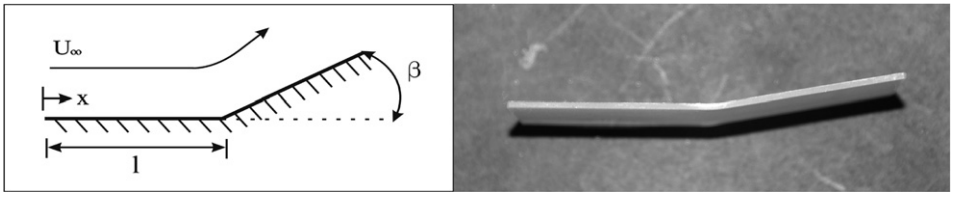

Fig. 9. Geometry of plate-wedge flow and a photograph of glass with naphthalene coating.

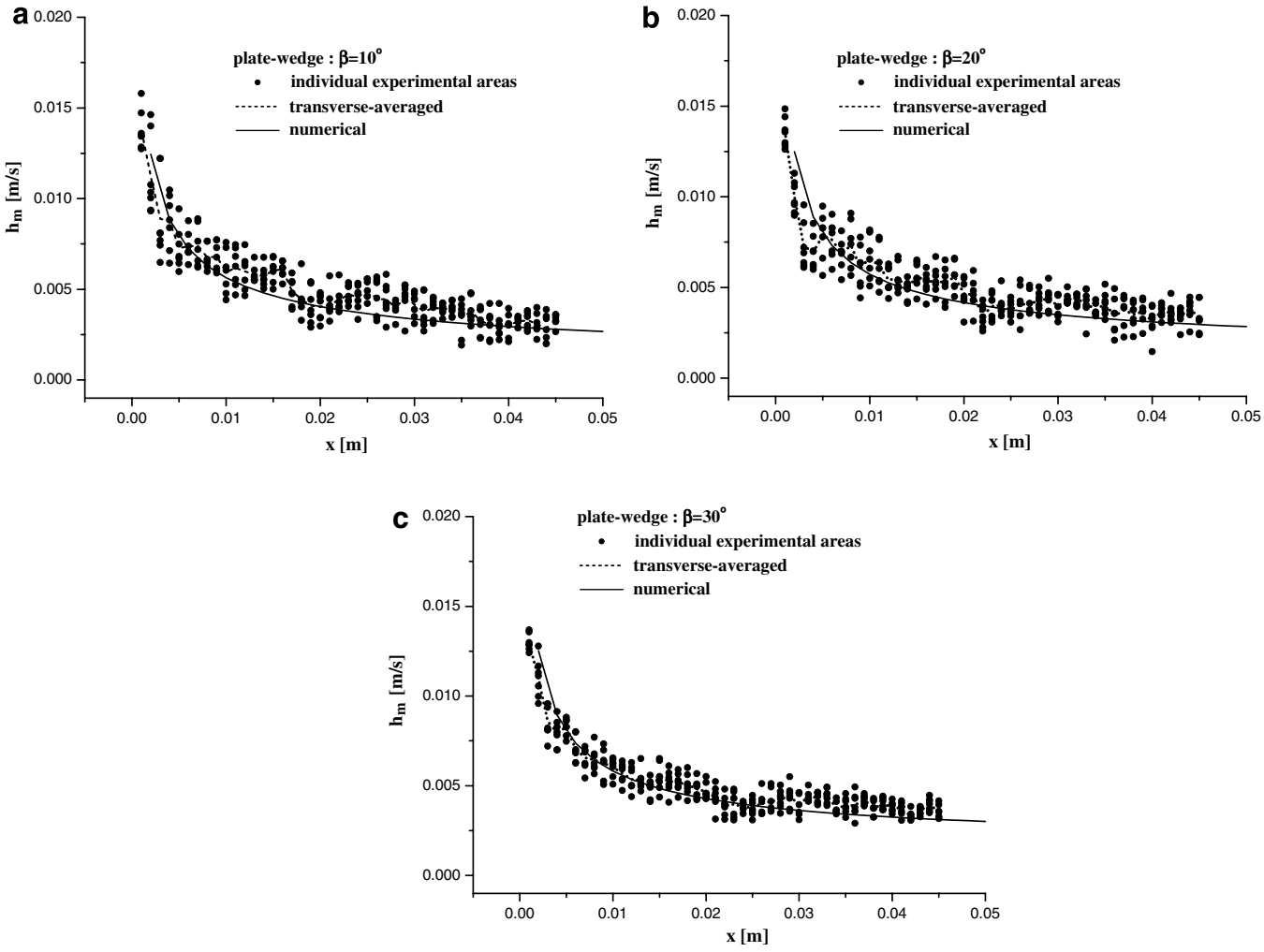

Fig. 10. Comparison between the experimental results and the numerical solutions for the plate-wedge flow. (a) Angle of the wedge $\beta = 10°$, (b) angle of the wedge $\beta = 20°$, (c) angle of the wedge $\beta = 30°$.

we consider each of the sampling areas, and the accuracy is greatly improved when the nine transverse data are averaged. The case of 180°, i.e., an impinging flow, is characteristic of a uniform mass transfer coefficient along the flow direction. The experimental results are in good agreement with the analytic exact solution again with the total uncertainty of 9.3%.

The third experiment is combination of flat plate and wedge flows. The glass substrate is made in a bent shape. Fig. 9 shows the geometry of the plate-wedge shape and the real glass substrate with naphthalene coating. The leading flat plate is 2.5 cm long (λ) and wedge part starts from the end of the leading part. The experiments are carried out varying the wedge angle β. The transformed x-momentum equation [15] obtained from the boundary-layer equation using similarity variable is solved numerically by a fourth-order Runge-Kutta procedure [16]. Comparison between the experimental results and the numerical ones is shown in Fig. 10. The experimental results for cases of 10°, 20° and 30° are all in fair agreement with the numerical results.

The last experiment is for the flow around a circular cylinder. The experimental results about this flow have been reported by many researchers. The reference data to be compared with this experiment is taken from Krall and Eckert [12]. Cylinder diameter D is 0.02 m and the Reynolds number is 1630. A half cylinder of glass, while the other is perfectly symmetric, is taken and naphthalene is coated on it. Later, the laser light is projected on to the outer surface and the optical signal is measured from inside. Fig. 11 shows the experimental results contrasted to the reference. Note that the optical images are taken at continuously varying oblique angle. Since the light of laser is perpendicularly irradiated to the cylinder and the CCD camera takes images in a horizontal position while the glass cylinder has a thickness of 2 mm and the correlation between the light intensity and the naphthalene thickness is indiscernible over incidence angle of 80°, it is difficult to obtain meaningful images below 40° and above 130°. The results are consequently shown for 40–130°. Both of the two experimental results are in good agreements.

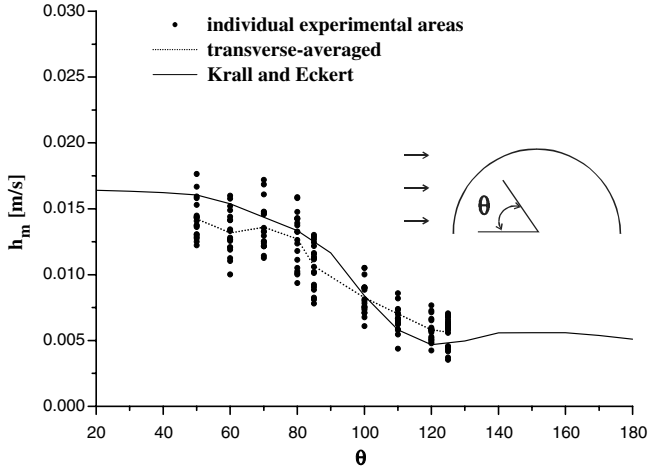

Fig. 11. Comparison between the experimental results and that of Krall and Eckert [12] for the circular cylinder flow.

These examples prove the validity of the proposed optical method. It can be applied complicated geometries with relative ease. The uncertainty is less than 10%, and it can be further improved by taking more sampling areas which are not closely located. Indeed, new methods of obtaining finer or less-correlated grains can be devised to achieve even higher experimental accuracy.

5. Conclusion

In the present work, a new measurement technique of naphthalene thickness using optical method is presented for application to complicated geometries. A novel coating method with vacuum chamber is proposed and tested to prove its applicability. The surface of naphthalene has fine surface and uniform thickness. The correlations between the naphthalene thickness and the optical image strength detected at the back of coating are obtained. The light intensity decreases with the large incidence angle and the thick naphthalene coating.

Wind tunnel experiments are performed to actually demonstrate the application of the optical method. Experiments with flat plate, wedge, plate-wedge and circular cylinder flow are made to compare with reference solutions. The experimental results show that the presented measurement is found to be accurate with an uncertainty of less than 10% and is applicable to complicated geometries which are difficult to cast the naphthalene. The accuracy can be further improved by taking more transverse samples.

References

[1] F.E.M. Saboya, E.M. Sparrow, Local and average transfer coefficient for one-row plate fin and tube heat exchanger configurations, ASME J. Heat Transfer 96 (1974) 265–272.
[2] M.K. Chyu, Heat transfer and pressure drop for short pin–pin arrays with pin-endwall fillet, J. Heat Transfer 112 (1990) 926–932.
[3] S.B.H.C. Neal, E.W. Northover, J.A. Hitchcock, The development of a technique for applying naphthalene to surface for mass transfer analogue investigations, J. Phys. E Sci. Instrum. 3 (1970) 636–638.
[4] S.B.H.C. Neal, The development of the thin-film naphthalene mass-transfer analogue technique for the direct measurement of heat-transfer coefficients, Int. J. Heat Mass Transfer 18 (1975) 559–567.
[5] Y.N. Lee, Heat transfer and pressure drop characteristics of an array of plates aligned at angles to the flow in a rectangular duct, Int. J. Heat Mass Transfer 29 (1986) 1553–1563.
[6] Y.N. Lee, Heat transfer and pressure drop characteristics of an assembly of partially segmented plates, J. Heat Transfer 111 (1989) 44–50.
[7] E.M. Sparrow, J.W. Ramsey, Heat transfer and pressure drop for a staggered wall-attached array of cylinders with tip clearance, Int. J. Heat Mass Transfer 21 (1978) 1369–1377.
[8] Y.H. Zhang, L.B. Wang, F. Ke, Y.X. Su, S.D. Gao, The effects of span position of winglet vortex generator on local heat/mass transfer over a three-row flat tube bank fin, Int. J. Heat Mass Transfer 40 (2004) 881–891.

[9] J.H. Park, S.Y. Yoo, A naphthalene sublimation study on heat/mass transfer for flow over a flat plate, KSME Int. J. 18 (7) (2003) 1258–1266.
[10] J.Y. Kim, T.H. Song, Effect of tube alignment on the heat/mass transfer from a plate fin and two-tube assembly: naphthalene sublimation results, Int. J. Heat Mass Transfer 46 (2003) 3051–3059.
[11] R.J. Goldstein, H.H. Cho, A review of mass transfer measurements using naphthalene sublimation, Exp. Therm. Fluid Sci. 10 (1995) 416–434.
[12] K.M. Krall, E.R.R. Eckert, Local heat transfer around a cylinder at low Reynolds number, J. Heat Transfer 95 (1973) 273–275.
[13] F.P. Incropera, D.P. Dewitt, Fundamentals of Heat and Mass Transfer, fourth ed., John Wiley & Sons, New York, 1996.
[14] T.G. Beckwith, R.D. Marangoni, J.H. Lienhard, Mechanical Measurements, fifth ed., Addison-Wesley, New York, 1993.
[15] L.C. Burmeister, Convective Heat Transfer, John Wiley & Sons, New York, 1993.
[16] J.D. Hoffman, Numerical Methods for Engineers and Scientists, Int. ed., McGraw-Hill, New York, 1993.
[17] J.P. Holman, Experimental Methods for Engineering, Addison-Wesley, New York, 1993.